ChemPubSoc Europe

DOI: 10.1002/chem.201701029

CHEMISTRY
A European Journal
Full Paper

Noncovalent Interactions

Supramolecular Hydrogels Based on Minimalist Amphiphilic Squaramide–Squaramates for Controlled Release of Zwitterionic Biomolecules

Carlos López, Marta Ximenis, Francisca Orvay, Carmen Rotger, and Antonio Costa*[a]

Abstract: Supramolecular hydrogels with tunable properties have innovative applications in biomedicine, catalysis, and materials chemistry. Minimalist low-molecular-weight hydrogelators based on squaramide and squaramic acid motifs have been designed. This approach benefits from the high acidity of squaramic acids and the aromaticity of squaramides. Moreover, substituents on the aryl ring tune the π density of the arylsquaramide motif. Thus, materials featuring distinct thermal and mechanical properties have been successfully prepared. The hydrogel ($G' \approx 400$ Pa, $G'' \approx 57$ Pa; at 1.0% w/v; 1 Hz) obtained from 4-nitrophenylsquaramide motif **1** is thermoreversible ($T = 57\,^{\circ}C$ at 0.2% w/v), thixotropic, self-healable, and undergoes irreversible shrinking in response to saline stress. Furthermore, the hydrogel is injectable and can be loaded with substantial amounts (5:1 excess molar ratio) of zwitterionic biomolecules, such as L-carnitine, γ-aminobutyric acid (GABA), or D,L-Ala-D,L-Ala, without any loss of structural integrity. Then, the release of these molecules can be modulated by saline solutions.

Introduction

Supramolecular hydrogels,[1] formed through the noncovalent assembly of low-molecular-weight hydrogelators (LMWHs), are materials of scientific interest for innovative applications in biomedicine,[2] catalysis,[3] and materials chemistry.[4] Because of their essential reversible character, water gelation by small molecules provides gel-to-sol transitions and a rapid response to external stimuli. Of equal importance, appropriate design and limited synthetic effort required in their preparation allow effective control over the assembled structures and their responses on the macroscopic level. This control is highly desirable for practical applications because it enables the creation of hydrogels with tunable mechanical properties.[1a]

Because of the complexity of the self-assembly phenomenon, the ex novo design of supramolecular hydrogels by using LMWHs is challenging. There is a consensus that LMWHs possess amphiphilicity and require noncovalent interactions, such as π–π, hydrogen bonding, and charge interactions, among the constituent molecules to build 3D networks in water.[5] Specifically, peptides and other amide-like compounds, which contain hydrophilic (charged) and hydrophobic side chains, have been successfully used as LMWHs.[1,6] In this vein, disecondary squaramides and squaramic acids are advantageous because they can establish synergic hydrogen-bonding/aromaticity relationships that control the outcome of the aggregation process[7] in the solid state[8] and in solution.[9] However, N-aryl-substituted squaramic acids[10] are highly acidic compounds ($pK_a = 0.8$–2) that have never been used for hydrogel construction. High acidity is crucial when using squaramic acids as the hydrophilic portion of an LMWH because the acidity ensures complete ionization over a broad pH range.[10a] As with the squaramides, squaramic acid salts (named squaramates) are moderately aromatic.[8b] Both arylsquaramides and arylsquaramates are planar and can form antiparallel stacked dimers in the solid state (Figure 1 a and b).[8b,11,12] Overall, the

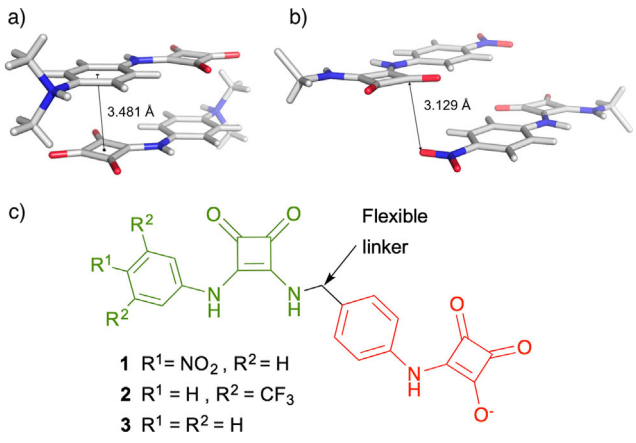

Figure 1. a) Partial X-ray structure illustrating the planar stacked-offset arrangement of the *p*-nitrophenylsquaramide motif.[12] b) X-ray structure of a phenylsquaramic acid.[8d] c) Chemical structures of amphiphilic squaramide–squaramic LMWHs **1**–**3**.

[a] C. López, M. Ximenis, F. Orvay, Prof. C. Rotger, Prof. A. Costa
Departament de Química, Facultad de Ciències
Universitat de les Illes Balears
Ctra. Valldemossa, Km. 7.5, Palma 07122 (Spain)
E-mail: antoni.costa@uib.es

Supporting information and the ORCID identification number(s) for the author(s) of this article can be found under https://doi.org/10.1002/chem.201701029. It contains full details of synthetic and experimental procedures.

hydrolytic stability[13] and aggregation capabilities of squaramides and squaramates renders their use as synthons for LMWH attractive.

Inspired by the solid-state structures of reported squaramide derivatives, we hypothesized that the combination of arylsquaramide and arylsquaramate motifs would enhance the stacking interactions of the resulting squaramide–squaramate ensemble (Figure 1c). Herein, we report that LMWHs based on the squaramide–squaramate couple (Figure 1) self-assemble to form supramolecular hydrogels. The role of the substituents $-NO_2$ and $-CF_3$ on the arylsquaramide moiety is intended to modulate the molecular aggregation of the LMWHs to tune the macroscopic properties of the resulting hydrogels.

Results and Discussion

We synthesized amphiphilic LMWHs **1**–**3**. Precursors **1**–**3** share a common squaramide–squaramate framework, but surprisingly show strikingly distinct aggregation properties in water. The addition of NaOH triggers the self-assembly and hydrogelation of **1** ($R^1 = NO_2$; $R^2 = H$) in minutes at a pH range of 3–9, with or without heating. The resulting hydrogel **1A** passes the vial inversion test at a relatively low concentration (0.1–0.2% w/v; Figure 2a).

Similarly, squaramide **2** ($R^1 = H$; $R^2 = CF_3$) also gels, but requires heating to obtain the hydrogel, and the critical gelation concentration is higher (1.6% w/v; Figure 2b and Table S1 in the Supporting Information). However, after similar treatment, squaramide **3** remains as a suspension, even with extensive sonication and heating. A comparison of the AFM images of freshly prepared samples of hydrogels **1A** and **2A** (Figure 2e and f, respectively) reveals marked morphologic differences. Aside from the micrometer-sized disordered fibers observed in the two hydrogels, hydrogel **1A** shows bundled fibrous assemblies composed of one or more strands with an apparent width of 42 nm (2 nm height; Figure S1 in the Supporting Information). Meanwhile, the morphology of **2A** comprises both right- and left-handed helical ribbons with an average diameter of 52 nm twisting around the central axis of the fiber (Figure 2g–j and Figure S2 in the Supporting Information). SEM and TEM images of dried samples of hydrogels **1A** and **2A** confirm the formation of networks of bundled fibers characteristic of hydrogels (Figure 2c and d and Figures S3 and S4 in the Supporting Information). Undoubtedly, different morphologies of hydrogels **1A** and **2A** and the failure of hydrogel formation of precursor **3** reflect the influence of peripheral substituents on the self-assembly of the precursor hydrogelators.

To shed light on the initial self-assembly events, we studied the evolution of the ^1H NMR spectra of solutions of **1** (1.0×10^{-3} M) in different solvent mixtures of [D6]DMSO/H_2O. Upon increasing the amount of water in the solvent mixture, all aromatic protons exhibit significant upfield shifts (−0.1 to −0.5 ppm), which indicates the growing influence of the aromatic stacking interactions that occur in water (Figure 3). Previously, we have reported that a dynamic equilibrium driven by hydrogen bonding between the mono- and dimeric forms of **1** exists in [D6]DMSO.[14] In agreement with this, the NH proton

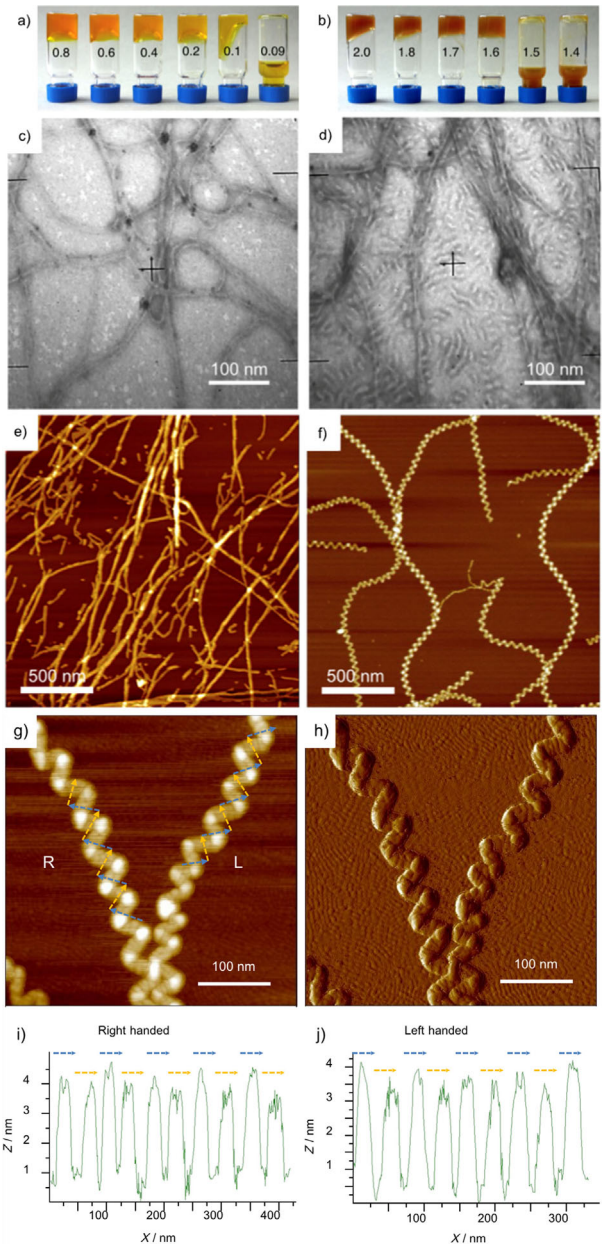

Figure 2. Vial inversion tests performed on slow-cooled samples of **1A** (a) and **2A** (b), after gentle heating at 70 °C for 1 h. The values on the vials indicate the percentage (w/v) of the hydrogelators **1** and **2**. TEM images of fibrils from the self-assembly of **1A** (b; 0.03% w/v; $c = 0.58$ mM) and **2A** (c; 0.018% w/v; $c = 0.41$ mM) in water. The hydrogels were negatively stained with 1% (w/v) phosphotungstic acid before observation. AFM images obtained on mica by depositing 60 μL aliquots of diluted hydrogels **1A** (e; 0.015% w/v; $c = 0.34$ mM) and **2A** (f; 0.015% w/v; $c = 0.29$ mM). g) Enlarged image of two helices, one right-handed (R) and another left-handed (L), and its corresponding amplitude image (h). i) and j) Cross-section profiles plotted following the dashed lines in g) indicating the direction of rotation of the two helices. The colors of the dashed arrows on each peak are referenced to the corresponding fragment of the cross section.

of the squaramate first moves downfield and then reverses direction, which indicates hydrogen-bond breaking, in DMSO/H_2O mixtures containing $>50\%$ H_2O.

HRMS (ESI(−)) analysis of very dilute solutions of **1**–**3** ($c \approx 10^{-6}$ M) also provides clues about the aggregation of these

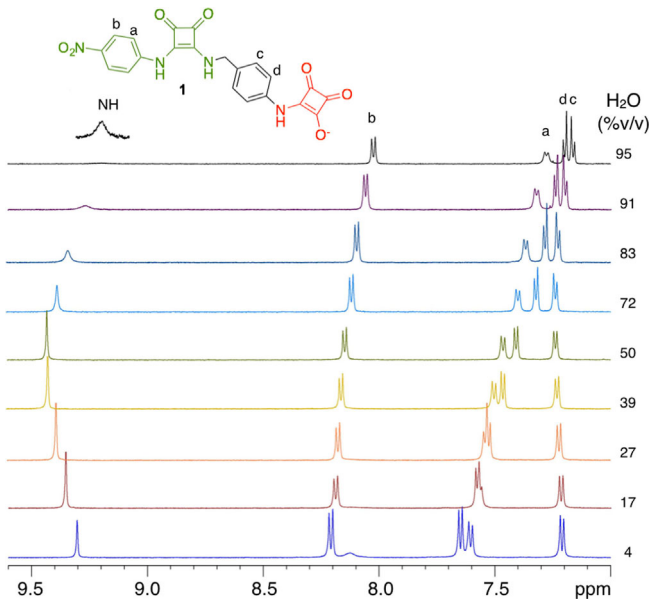

Figure 3. Partial ^{1}H NMR spectra (300 MHz) of a solution of the sodium salt of **1** (1.0×10^{-3} M) at room temperature in mixtures of [D6]DMSO/H_2O containing increasing percentages of H_2O. All spectra were registered by using WATERGATE pulse sequences for water suppression.

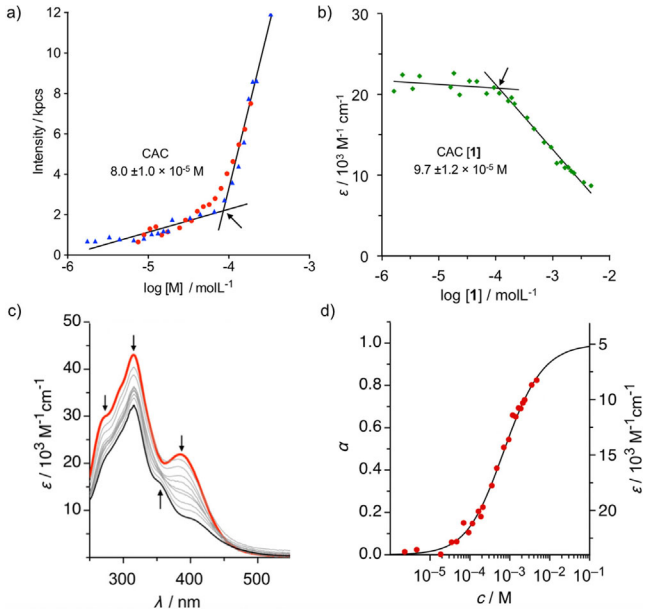

Figure 4. a) Scattered intensity [s^{-1}] as a function of concentration, log [M], of **1** (red) and **2** (blue). b) Molar extinction coefficients of **1** at $\lambda = 390$ nm as a function of the concentration of **1**. In both cases, the calculated critical aggregation concentration (CAC) at the line junctions are indicated on the plots. c) Concentration-dependent UV/Vis spectra of hydrogel **1 A** obtained over a concentration range from 4.6×10^{-5} (red) to 7.0×10^{-3} M (black). The arrows indicate the direction of movement upon increasing the concentration of **1 A**. d) Molar fraction (α) of aggregated molecules as a function of concentration of **1 A**. The line was obtained by fitting the experimental UV/Vis data with the isodesmic model.

precursors. Squaramide **1** shows an intense base signal at *m/z* 433.0789 assigned to the monomer $[M-H]^-$ anion with 44% contribution of the doubly charged dimer, $[2M-2H]^{2-}$. The base signal of **2** appears at *m/z* 524.0681 and the contribution of the dimer increases to 68%. In both cases, several minor signals at higher *m/z* assigned to low oligomers were also observed, albeit at a proportion <5% compared with that of the dimer. In contrast, the molecular signal of **3** at *m/z* 389.3670 contains less than 3% of the dimer; thus indicating the low aggregation ability of **3** (Figures S5–S7 in the Supporting Information).

The formation of aggregates from **1** and **2** was assessed by static light scattering (SLS) and UV/Vis measurements. A plot of scattered intensity as a function of concentration displays almost superimposable curves for the two hydrogels (Figure 4a). From these data, the CAC for the two hydrogels calculated at the junction is $(8.0\pm1.0\times10^{-5})$ M, which is similar to that found by UV/Vis for **1** (Figure 4b). However, the change between the two lines is not as abrupt as one would expect for a cooperative aggregation model.

To gather further information, we explored the aggregation of hydrogel **1 A** by UV/Vis. Hydrogelator **1**, which is more soluble than **2**, allows aggregation equilibria to be studied over a broader range of concentrations.

The UV/Vis spectra of solutions of **1** in water, registered below the CAC, do not show isosbestic points that indicate the absence of other equilibria, namely, acid–base.[12a,15] The high-intensity band at $\lambda = 318$ nm is common to all squaramide and squaramic derivatives, and hence,[10] its diagnostic value is minimal. The lowest energy band appears at $\lambda \approx 388$ nm (Figure 4c), which we assigned to the S_0–S_1 electronic transition of the 4-nitrophenylsquaramide chromophore. Upon increasing the concentration of **1**, the band at $\lambda = 388$ nm vanishes completely, and a new band appears blueshifted as a shoulder at $\lambda = 355$ nm, which suggests H aggregation. Remarkably, the band at $\lambda = 388$ nm reappears upon heating (Figure S9 in the Supporting Information); thus indicating the reversible character of aggregation and providing clear evidence that the aggregation of **1** involves electronic interactions between the 4-nitrophenylsquaramide chromophores. In agreement, the apparent molar absorption coefficient at $\lambda = 388$ nm could be fitted to the isodesmic (equal K) model of aggregation (Figure 4d), producing an association constant of (800 ± 75) M^{-1}, which compares well with published values.[16]

The phenyl substituents of **1** ($-NO_2$) and **2** ($-CF_3$) not only modify the initial hydrogel core formation capabilities, but strongly influence their responsiveness to external stimuli, such as heat and shear. We analyzed the thermal behavior of hydrogels **1 A** and **2 A** by differential scanning calorimetry (DSC) and the vial inversion method (Table S2 in the Supporting Information). A DSC thermogram of **1 A** (0.25% w/v) from 25–90 °C (Figure S10 in the Supporting Information) exhibits an endothermic peak at $T = 57$ °C. The peak is dependent on concentration and its broad shape reveals the continuous character of the transitions that occur in the hydrogel. Moreover, the hydrogel is thermoreversible, that is, it evolves into solution upon heating and then returns to the hydrogel form upon cooling at room temperature. In contrast, the DSC thermogram of **2 A** registered over the same temperature range displays a flat line, which indicates that hydrogel **2 A** is thermally stable.

We confirmed the hydrogel nature of **1A** and **2A** by conducting dynamic rheological experiments. The frequency-sweep experiments show a value of the storage modulus (G') 10-fold greater than that of the loss modulus (G'') over the entire frequency range (1% strain; frequency range 0.1–100 Hz); this is characteristic of viscoelastic fibrous networks (Figure S13 in the Supporting Information). At the same concentration (2% w/v), the magnitude of the G' modulus for **2A** is ten times greater than that for **1A**; thus demonstrating its greater resistance against mechanical disturbance.

To evaluate the biocompatibility of **1**, U87 cells were subconfluently grown in the presence of hydrogelator **1** at increasing concentrations. The toxicity was evaluated by a luminescent test. No toxicity was found for concentrations of **1** up to 500 μM (Figure S11 in the Supporting Information). Thus, the lack of toxicity and weak stacking interactions that govern the structure of **1A** translate into a set of properties of high interest for biotechnological applications. In addition to being thermoreversible at a relatively low temperature, hydrogel **1A** is thixotropic (its viscosity diminishes under compression); therefore, hydrogel **1A** flows into small channels and it is readily injectable (Figure 5b). We assessed the thixotropic behavior of **1A** by applying stepwise cycles of high and low stress to a sample of **1A** (2% w/v; Figure 5a). Under low strain, the hydrogel displays a storage modulus an order of magnitude higher than that of the loss modulus, which is consistent with its gel state. At high strain, both storage and loss moduli drop to reach similar values, indicating a phase transition from a gel to a solution.[17] The application of low strain allowed the moduli to recover rapidly the same magnitudes as those observed before the stress.

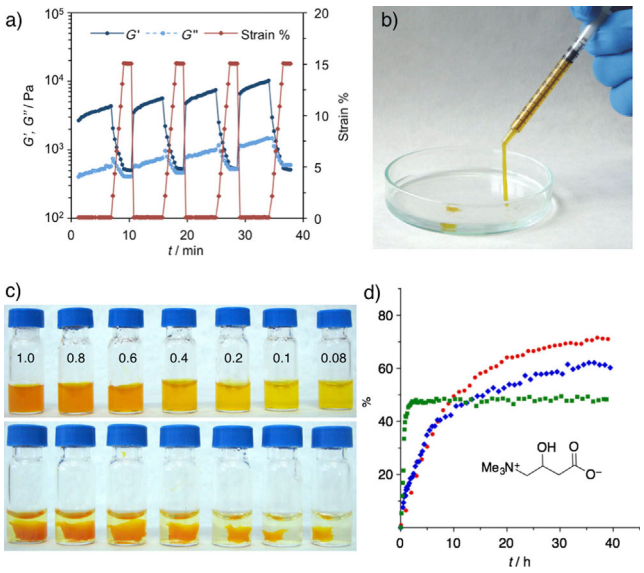

Figure 5. a) Rheology time sweep of **1A** (2% w/v) at 1 Hz by applying four cycles of low (0.1%, 6 min) and high strain (15%, 90 s) at 25 °C. b) Photograph of hydrogel **1A** (1.0% w/v; 1 Hz; $G' \approx 400$ Pa, $G'' \approx 57$ Pa), indicating the fluid-like properties. c) Photographs of **1A** (500 μL) before and after the addition of a solution of NaCl (50 μL, 50 mM) showing shrinking at equilibrium (24 h). The concentration of **1A** (% w/v) is labeled on the vials. d) Comparative release profile of L-carnitine (69 mM) loaded in **1A** (0.6% w/v, 100 μL) at 25 °C and covered by 500 μL of water (red) or 100 (blue) and 300 mM NaCl (green).

When dipped in water, the hydrogel remains unaltered for weeks. However, the addition of saline solutions (such as NaCl, Et_4NCl, KCl, $MgCl_2$, Me_4NOAc, or acetylcholine chloride) to **1A** causes homogeneous and irreversible shrinking, in such a way that the shrunken gel keeps the shape of its container. The magnitude of the macroscopic phase transition depends on the total concentration of salt added and its molar ratio to the hydrogelator (Figure 5c and Figure S12 in the Supporting Information). The kinetics of the process is fast because, after 4 h from the addition of the salt solution, the hydrogel shrinks to essentially its final volume. When completely shrunken, the stiffness of the resulting hydrogel **1B** increases considerably relative to that of **1A** (1 Hz, $G'_{1B}/G'_{1A} \approx 25$, $G''_{1B}/G''_{1A} \approx 20$; Figure S14 in the Supporting Information).

Finally, in contrast to the shrinking effect of added salts, hydrogel **1A** can be loaded with a variety of zwitterionic molecules, such as L-carnitine, γ-aminobutyric acid (GABA), and D,L-Ala-D,L-Ala, without disturbing the hydrogel structure. These molecules can be added in a 5:1 excess molar ratio to **1**, before heating, without disturbing the mechanical stability of the resulting loaded hydrogel. However, the addition of related organic salts, such as tetramethylammonium acetate or acetylcholine chloride, to the solution of **1** causes shrinking of the hydrogel.

The loaded hydrogel can release the zwitterions in a controlled manner upon covering the hydrogel with water (Figure 5d). Depending on the compound used as a payload, 30–70% of the zwitterion is released into water in less than 24 h.

Alternatively, stimulated release is observed in the presence of saline solutions with a concomitant reduction in the total amount discharged. Thus, although 47% of L-carnitine is released in water within 10 h, in a 0.3 M solution of NaCl, the same amount is reached in 2 h; in this case, part of the payload remains entrapped in the shrunken hydrogel. In all cases tested, the release follows a pseudo-second-order kinetic model, which is characteristic of solid–liquid sorption processes (Figure S15 in the Supporting Information).

The above experiments highlight the structural, thermal, and mechanical differences existing between hydrogels **1A**, **1B**, and **2A**. These differences arise from different contributions of the arylsquaramide substituents. The results obtained provide clear evidence that parallel stacking of the 4-nitrophenylsquaramide governs the aggregation of **1** to **1A**. However, the two CF_3 substituents of the 3,5-bistrifluoromethylphenylsquaramide can establish additional C_{Ar}–H···F–C(sp^3) and C(sp^3)–F···F–C(sp^3) interactions. In addition to aromatic stacking, fluorine interactions are likely to contribute to the aggregation of **2**, as observed in the solid-state structure of a related squaramide derivative.[13b]

Conclusion

We have demonstrated the formation of hydrogels based on squaramide–squaramate ensembles. We have utilized squaramic acids, for the first time, as the hydrophilic component of

minimalist LMWHs, joined to an arylsquaramide unit as the hydrophobic moiety. The aryl substituents (NO_2 and CF_3) induce dramatic thermal and mechanical differences in the aggregation of the hydrogels. The hydrogel containing the 4-nitrophenylsquaramide motif is thermoreversible, thixotropic, injectable, and can be loaded with a substantial amount of zwitterionic biomolecules, which are rarely used as payloads. Overall, we have demonstrated the technological potential of the squaramide–squaramate couple as a new tool for the design of supramolecular hydrogels.

Acknowledgements

We thank the Ministry of Economy and Competiveness for financial support (grant ref. CTQ2014-57393-C2-1-P) and C.L. thanks the Government of the Balearic Islands (CAIB) and European Social Funds (FSE) for a predoctoral fellowship. We thank Dr. G. Martorell and Dr. R. Gomila (SCT-UIB) for assistance with HRMS measurements, and Prof. Priam Villalonga and Dr. Guillem Ramis for evaluation of cytotoxicity.

Conflict of interest

The authors declare no conflict of interest.

Keywords: gels · noncovalent interactions · squaramides · supramolecular chemistry · zwitterions

[1] a) M. J. Webber, E. A. Appel, E. W. Meijer, R. Langer, *Nat. Mater.* **2015**, *15*, 13 – 26; b) R. Dong, Y. Pang, Y. Su, X. Zhu, *Biomater. Sci.* **2015**, *3*, 937 – 954; c) D. Yuan, B. Xu, *J. Mater. Chem. B* **2016**, *4*, 5638 – 5649; d) M. D. Segarra-Maset, V. J. Nebot, J. F. Miravet, B. Escuder, *Chem. Soc. Rev.* **2013**, *42*, 7086 – 7098; e) X. Du, J. Zhou, J. Shi, B. Xu, *Chem. Rev.* **2015**, *115*, 13165 – 13307.

[2] For recent examples, see: a) E. V. Alakpa, V. Jayawarna, A. Lampel, K. V. Burgess, C. C. West, S. C. Bakker, S. Roy, N. Javid, S. Fleming, D. A. Lamprou, *Chem.* **2016**, *1*, 298 – 319; b) H. Shigemitsu, T. Fujisaku, S. Onogi, T. Yoshii, M. Ikeda, I. Hamachi, *Nat. Protoc.* **2016**, *11*, 1744 – 1756.

[3] N. Singh, K. Zhang, C. A. Angulo-Pachón, E. Mendes, J. H. van Esch, B. Escuder, *Chem. Sci.* **2016**, *7*, 5568 – 5572.

[4] M. D. Konieczynska, J. C. Villa-Camacho, C. Ghobril, M. Perez-Viloria, K. M. Tevis, W. A. Blessing, A. Nazarian, E. K. Rodriguez, M. W. Grinstaff, *Angew. Chem. Int. Ed.* **2016**, *55*, 9984 – 9987; *Angew. Chem.* **2016**, *128*, 10138 – 10141.

[5] a) L. A. Estroff, A. D. Hamilton, *Chem. Rev.* **2004**, *104*, 1201 – 1218; b) S. S. Babu, V. K. Praveen, A. Ajayaghosh, *Chem. Rev.* **2014**, *114*, 1973 – 2129.

[6] a) Y. Li, F. Wang, H. Cui, *Bioeng. Transl. Med.* **2016**, *1*, 306 – 322; b) J. W. Steed, *Chem. Soc. Rev.* **2010**, *39*, 3686 – 3699; c) Y. Wan, Z. Wang, J. Sun, Z. Li, *Langmuir* **2016**, *32*, 7512 – 7518; d) R. Liang, Z. Luo, G. Pu, W. Wu, S. Shi, J. Yu, Z. Zhang, H. Chen, X. Li, *RSC Adv.* **2016**, *6*, 76093 – 76098.

[7] V. Saez Talens, P. Englebienne, T. T. Trinh, W. E. Noteborn, I. K. Voets, R. E. Kieltyka, *Angew. Chem. Int. Ed.* **2015**, *54*, 10502 – 10506; *Angew. Chem.* **2015**, *127*, 10648 – 10652.

[8] a) A. Portell, M. Font-Bardia, R. Prohens, *Cryst. Growth Des.* **2013**, *13*, 4200 – 4203; b) R. Prohens, A. Portell, M. Font-Bardia, A. Bauzá, A. Frontera, *Cryst. Growth Des.* **2014**, *14*, 2578 – 2587; c) C. Estarellas, M. C. Rotger, M. Capó, D. Quiñonero, A. Frontera, A. Costa, P. M. Deyà, *Org. Lett.* **2009**, *11*, 1987 – 1990; d) C. Rotger, B. Soberats, D. Quiñonero, A. Frontera, P. Ballester, J. Bene *t*Buchholz, P. M. Deyà, A. Costa, *Eur. J. Org. Chem.* **2008**, 1864 – 1868.

[9] a) B. Soberats, L. Martínez, E. Sanna, A. Sampedro, C. Rotger, A. Costa, *Chem. Eur. J.* **2012**, *18*, 7533 – 7542; b) J. Schiller, J. V. Alegre-Requena, E. Marqués-López, R. P. Herrera, J. Casanovas, C. Alemán, D. Díaz Díaz, *Soft Mater.* **2016**, *12*, 4361 – 4374.

[10] Squaramic acid stands for 3-hydroxy-4-amino-cyclobut-3-ene-1,2-dione. a) C. López, M. Vega, E. Sanna, C. Rotger, A. Costa, *RSC Adv.* **2013**, *3*, 7249 – 7253; b) J. Xie, A. B. Comeau, C. T. Seto, *Org. Lett.* **2004**, *6*, 83 – 86.

[11] E. Sanna, L. Martínez, C. Rotger, S. Blasco, J. González, E. García-España, A. Costa, *Org. Lett.* **2010**, *12*, 3840 – 3843.

[12] M. Ximenis, E. Bustelo, A. G. Algarra, M. Vega, C. Rotger, M. G. Basallote, A. Costa, *J. Org. Chem.* **2017**, *82*, 2160 – 2170.

[13] a) V. Amendola, G. Bergamaschi, M. Boiocchi, L. Fabbrizzi, M. Milani, *Chem. Eur. J.* **2010**, *16*, 4368 – 4380; b) R. B. Elmes, P. Turner, K. A. Jolliffe, *Org. Lett.* **2013**, *15*, 5638 – 5641.

[14] C. López, E. Sanna, L. Carreras, M. Vega, C. Rotger, A. Costa, *Chem. Asian J.* **2013**, *8*, 84 – 87.

[15] X. Ni, X. Li, Z. Wang, J. P. Cheng, *Org. Lett.* **2014**, *16*, 1786 – 1789.

[16] Z. Chen, A. Lohr, C. R. Saha-Möller, F. Würthner, *Chem. Soc. Rev.* **2009**, *38*, 564 – 584.

[17] H. Ye, C. Owh, X. J. Loh, *RSC Adv.* **2015**, *5*, 48720 – 48728.

Manuscript received: March 6, 2017

Accepted Article published: April 4, 2017

Final Article published: ■■ ▮▮, 0000

FULL PAPER

Noncovalent Interactions

*C. López, M. Ximenis, F. Orvay, C. Rotger, A. Costa**

■■ – ■■

Supramolecular Hydrogels Based on Minimalist Amphiphilic Squaramide–Squaramates for Controlled Release of Zwitterionic Biomolecules

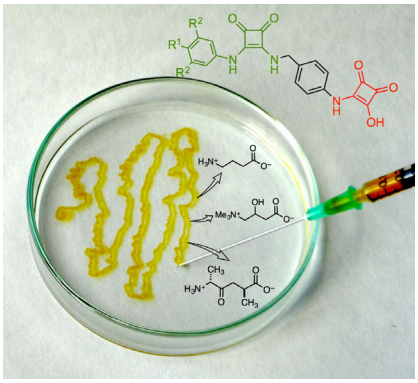

Drop the payload! Smart supramolecular hydrogels based on squaramides and squaramate synthons are thermoreversible, thixotropic, and injectable. These hydrogels can be loaded with zwitterions and display ion-stimulated shrinking and release of the payload (see figure). This combination of properties is unusual in supramolecular hydrogels derived from low-molecular-weight hydrogelators.